



Blast Load on Honeycomb Rigid Wall

Qiming Zhao*, Shou Chen, Hao Sun, Yun Wang

Department of Military Facilities, Army Logistics University of PLA, Chongqing 401331, China

Corresponding Author Email: frankchao404@gmail.com

<https://doi.org/10.18280/ijht.380227>

Received: 18 December 2019

Accepted: 6 March 2020

Keywords:

honeycomb-section, blast load prediction, blast experiment, numerical simulation

ABSTRACT

Blast wave and its reflected pressure distribution on rigid wall surface developed by a blast shockwave mainly depend on the section geometry of blast wall, and has always been key research topics of structural protection engineering and impact engineering. The current research mainly focuses on the wall with regular rectangular cross-section, but there has been little research on the blast load distribution of the honeycomb rigid wall subjected to blast wave. In this paper, a theoretical analysis has been carried out attempting to predict clearing blast load and reflected pressure distribution on honeycomb-section wall subjected to ground blast. Then, combined with LS/DYNA FEA method, a numerical simulation of blast load and shockwave propagation on honeycomb-section wall was carried out, and the blast experiment was conducted to verify the finite element model. The results indicated that the distribution of blast load on honeycomb wall presents a non-monotonic change along the length of the wall, and the incidence angle at blast surface of honeycomb wall periodically changes with the longitudinal direction of the wall, resulting in a sawtooth wave form of reflected pressure, and gradually decreasing with the increase of the distance between the measuring points along the wall length; The blast load predicting model of honeycomb established in this paper can reasonably reveal the overpressure distribution characteristics on blast wall of honeycomb-section rigid wall which has been verified by numerical simulation and blast experiment results. The research findings pave the way for studying the interaction between blast waves and the honeycomb-section wall in the explosion field, and provide supports for the prediction of the honeycomb-section wall blast load and protection design in impact engineering.

1. INTRODUCTION

With the gradual increase of the city size and population density around the world, any explosion near the densely populated urban structures will pose a serious threat to social public property and urban residents. On July 7, 2005, a terrorist attack on the London Underground occurred. The explosive blast acted on the surface of the station structure, resulting in varying degrees of damage to the underground station of London Liverpool Street and other building structures, and seriously affecting the normal operation of London urban rail transit and the safety of urban residents. Therefore, the in-depth study should be conducted about the overpressure distribution law of the explosion blast wave on the blast surface of the structural wall, which is of great significance for understanding the propagation mechanism of the blast wave against the structure wall during the explosion.

When the blast wave acts on the surface of the structural wall and is reflected, theoretically, the wall will deform under the action of overpressure. Ngo et al. [1] measured the relationship between the reflection of the explosion blast wave against the wall and the wall deformation response through field tests, and found that the two were not synchronized; Wu and Hao [2] used numerical simulation to study the reflection process of blast wave on the structural column and its deformation response, concluding that the shock reflection process on the structural column was not coupled with the structural deformation, and the deformation response of the

structural column always lagged behind the reflection process. For this, the authors assumed that the wall impacted by the blast wave is a rigid wall in this paper.

Rigby et al. evaluated the effect of blast wave clearing on the dynamic displacement of deformable finite targets, however the mechanism of blast wave clearing and loads for finite honeycomb rigid wall has not yet been fully explored [3-5]. Shoja et al. [6] calculated the pressure histories applied on structures considering the non-uniform loading characteristic as well as pressure relief from the edges, then the effects of various parameters on uniformity of impulse distribution are investigated. By using ANSYS/Autodyn, Qasrawi and Heffernan [7] proposed a tool to aid the blast resistant design engineer in more accurately quantifying the cleared blast loads imparted on a structure or structural element with a given distance from the edge. Rose et al. respectively applied CONWEP and CONWEP LOS to simulate the blast overload against the regular rigid wall with a finite boundary, and performed verification by an explosion test [8-11]. Rigby et al. [12] investigated the blast pressure load acting on finite targets where the presence of a free edge is known to cause a clearing wave to travel across the loaded face, new observations on the mechanism of blast wave clearing, and provides evidence to question the validity of methods for predicting clearing that exist in the current literature.

Rickman and Murrell [13], based on the CONWEP, conducted numerical simulation and a series of experimental studies on the blast wave pressure distribution of a small wall

structure with boundary effect, and found that the influence of the wall boundary shape on the wall reflection pressure cannot be ignored. Shi et al. [14] carried out a simulation study on the surface explosion blast wave distribution law of an independent circular cross-section column structure based on the finite element analysis (FEA) method, and proposed the calculation formulas for the explosion pressure, blast wave, and reflected pressure time-history on the independent structural column considering the effect of the cross-sectional shape.

Williams and Williamson [15] investigated the performance of highway bridges subjected to the nearby detonation of an explosive, especially focused on slender structural components in which the effects of cross-sectional geometry, engulfment of blast pressures, and clearing effects strongly influence loading history. Based on the findings obtained from the study, a simplified procedure for predicting blast loads acting against bridge columns is proposed. Liu et al. [16] established a high-fidelity finite element model of a pier-bent system for highway bridges, and Conventional Weapon Effects (CONWEP) reflected pressure on a rigid surface was applied directly on the structure surfaces. Study shows that CONWEP simplified blast loading may underestimate the blast-load effects to some extent.

At present, the experimental and numerical simulation studies on the blast wave overpressure distribution on the structure surface during the explosion mainly focus on the rigid wall with regular rectangular section, but there has been little research on the honeycomb wall. Especially, the experimental study of the interaction between the structure and blast wave at the wave gap between the honeycomb walls have not been carried out yet. As above, this paper takes the honeycomb rigid wall as the research object. A theoretical model of the peak load on the explosion surface considering the impact of the incident angle was established using the CONWEP method, and the blast wave propagation of the honeycomb wall was simulated by LS-DYNA. Finally, an explosion test was carried out to verify the theoretical distribution law and numerical analysis results.

2. THEORETICAL MODEL OF OVERPRESSURE DISTRIBUTION ON THE EXPLOSION SURFACE OF A HONEYCOMB RIGID WALL

When the blast wave encounters the blast wall in the air propagation process, it will be reflected on the blast wall. When the propagation direction of the blast wave front is perpendicular to the wall surface, the incident angle is 0° , i.e., regular reflection. In the case of regular reflection, the propagation direction of the reflected wave is opposite to the incident wave and perpendicular to the explosion surface, as shown on the left side of Figure 1.

Considering that the explosion blast wave in the air free field is perpendicularly incident on the blast wall at the propagation velocity D_1 , the initial state in incident wave front is p_0, ρ_0, u_0, e_0 , which respectively represent the initial pressure, initial density, particle velocity and specific internal energy; the state parameters behind the shock front are p_1, ρ_1, u_1, e_1 . From the continuity condition, it can be found that the parameters of the blast wave incident wave front and back have the following relationship:

$$\left. \begin{aligned} D_1 - u_0 &= \frac{1}{\rho_0} \sqrt{\frac{(p_1 - p_0) \rho_1 \rho_0}{\rho_1 - \rho_0}} \\ u_1 - u_0 &= \sqrt{(p_1 - p_0) \left(\frac{1}{\rho_0} - \frac{1}{\rho_1} \right)} \\ \frac{\rho_0}{\rho_1} &= \frac{0.4 p_1 \rho_0 + 2.4}{2.8 p_0 \rho_0} \end{aligned} \right\} \quad (1)$$

where, γ is the gas adiabatic index.

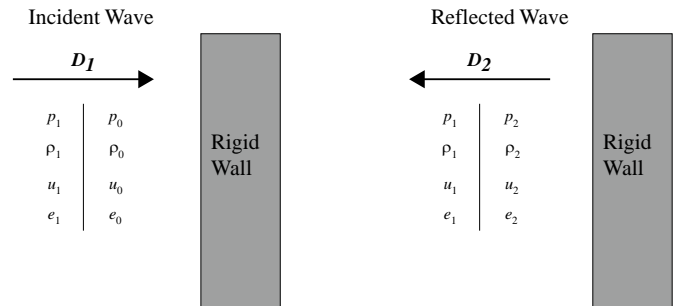


Figure 1. Regular reflection of explosion blast wave on the blast wall

When the incident wave front contacted the blast wall, the air velocity behind the wave front changed from u_1 to $u_2 = 0$. At this time, the kinetic energy of the gas medium behind the wave front was transformed into static pressure, so that the gas at the wall was compacted, the density increased from ρ_0 to ρ_1 , and the pressure changed from p_0 to p_1 , as shown on the right side of Figure 1.

Similarly, the parameter relationship between the blast wave front and back reflected on the blast wall can be derived as:

$$\left. \begin{aligned} D_2 - u_1 &= \frac{-1}{\rho_1} \sqrt{\frac{(p_2 - p_1) \rho_2 \rho_1}{\rho_2 - \rho_1}} \\ u_2 - u_1 &= -\sqrt{(p_2 - p_1) \left(\frac{1}{\rho_1} - \frac{1}{\rho_2} \right)} \\ \frac{\rho_1}{\rho_2} &= \frac{0.4 p_2 + 2.4 p_1}{0.4 p_1 + 2.4 p_2} \end{aligned} \right\} \quad (2)$$

Considering that the air mass point on the blast wall surface is initially static, that is, $u_0 = 0$, Equation (1) was combined with (2) to obtain:

$$\frac{p_2}{p_1} = \frac{(3\gamma - 1)p_1 - (\gamma - 1)p_0}{(\gamma - 1)p_1 - (\gamma + 1)p_0} \quad (3)$$

For the explosive blast wave, the incident peak overpressure was much greater than the atmospheric pressure, that is, $p_1 > p_0$, and then for the ideal gas, it's taken $\gamma = 1.4$, ignoring the influence of atmospheric pressure. Equation (3) shows that the reflected blast wave overpressure was about 8 times the incident overpressure. As the intensity of the incident blast wave increases, γ will be less than 1.4 due to the air dissociation, and the pressure on the reflected blast wave front is often greater than 8 times the incident overpressure. Thus,

the reflection phenomenon of the normal incident blast wave will greatly strengthen the failure and destruction of the blast wall.

Using the shock adiabatic, the pressure value of the regular reflection blast wave can be obtained according to the international standard of atmospheric pressure:

$$p_2 = 2p_1 + \frac{6p_1^2}{p_1 + 7.2} = \frac{8p_1^2 + 14p_1}{p_1 + 7.2} \quad (0.1MPa) \quad (4)$$

where, $p_1 \leq 4MPa$, and $2 \leq p_2/p_1 \leq 8$.

For the rigid front surface of a rectangular flat cross-section wall, the explosion blast wave can be approximately considered to be perpendicular vertically to the explosion blast wave, and the regular reflection pressure of the blast wall surface was obtained by formula (4). Thus, the approximate value of the blast load on the wall was obtained.

However, for the honeycomb wall, there is a corrugated concave-convex section shape along the length of the wall. When the explosion blast wave enters the implosion surface of the wall at a certain angle, complex oblique reflection occurs. In this case, using the normal reflection blast wave formula (4), it's estimated that the blast wave pressure distribution on the implosion surface may not match the actual project. Therefore, it is necessary to establish a theoretical model of the blast wave overpressure distribution on the rigid honeycomb wall.

CONWEP is an algorithm developed by the U.S. military to efficiently calculate the explosive load. Users can set the blast load of structural elements through simple settings. This algorithm does not simply convert the blast load into a triangular distribution peak overpressure, but calculates the peak overpressure load value acting on the structure through the position and angle of the explosion point and the target action surface.

The CONWEP algorithm is compiled and summarized by Kingery et al. [17] based on the US Army explosion test data. Then, Randers-Pehrson and Bannister [18] compiled blast simulation programs suitable for DYNA2D and DYNA3D on the strength of the CONWEP blast load model. When the incident blast wave reaches the surface of the structure and is reflected, the pressure P_L acting on the surface is the superimposition of the incident wave and the reflected wave, which can be considered to be the reaction force on the unit area of structural surface caused by the momentum change of the air medium on the surface of the structure. The pressure load acting on the structure surface was obtained by superimposing the reflected pressure value and the incident pressure value on the structure surface:

$$\left. \begin{aligned} P_L &= P_r \cos^2 \alpha + P_i (1 + \cos^2 \alpha - 2 \cos \alpha) \quad \cos \alpha \geq 0 \\ P_L &= P_i \quad \cos \alpha < 0 \end{aligned} \right\} \quad (5)$$

where, P_L is the blast wave pressure load per unit area; P_r and P_i are the blast wave (oblique) incident pressure and (perpendicular incident) reflected pressure at the unit area respectively; α is the angle between the incident pressure and the exterior normal outside the explosion surface of the structure, namely angle of incidence.

According to the experimental results, the impact of blast wave on the secondary incidence of the explosion surface was negligible, and the honeycomb rigid wall with circular cross-section took ABCD-A'B'C'D' as the calculation unit to remain

symmetrical, as shown in the yellow area in Figure 2. Then the y coordinate values of the ACC'A' plane and the DBB'D' plane are written as:

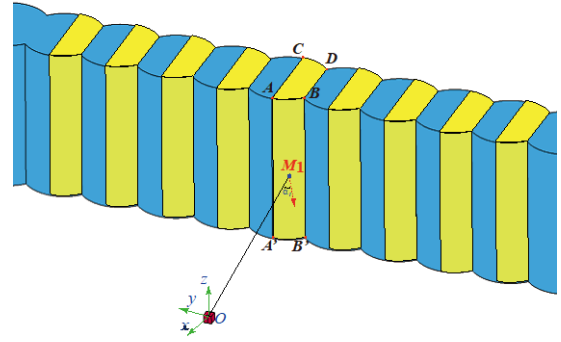


Figure 2. Division of calculation units in the honeycomb rigid wall

$$\left. \begin{aligned} y_{AC} &= \sqrt{2}kR \\ y_{BD} &= \sqrt{2} \left(k + \frac{1}{2} \right) R \end{aligned} \right\} \quad k = 0, \pm 1, \pm 2 \dots \quad (6)$$

Figure 2 shows that the normal vector of the blast surface at any point $M_1(x, y, z)$ of the calculation unit in the honeycomb wall can be expressed as:

$$\vec{n}_{M_1} = \left(\sqrt{R^2 - (y - \sqrt{2}kR)^2}, \quad y - \sqrt{2}kR, \quad 0 \right) \quad (7)$$

It's noted that the coordinates at the point $M_1(x, y, z)$ are related:

$$x = -D - R + \sqrt{R^2 - (y - \sqrt{2}kR)^2}$$

where, D is the component of the distance from the explosion center O to the explosion front face A on the x axis. Then the incident angle α_1 of the vector \vec{OM}_1 and the normal vector \vec{n}_{M_1} can be derived as:

$$\left. \begin{aligned} \cos(\alpha_1) &= -\cos \langle \vec{OM}_1, \vec{n}_{M_1} \rangle = -\frac{\vec{OM}_1 \cdot \vec{n}_{M_1}}{|\vec{OM}_1| |\vec{n}_{M_1}|} \\ &= -\frac{-(D+R)\sqrt{R^2 - (y - \sqrt{2}kR)^2} + R^2 - (y - \sqrt{2}kR)^2 + y^2 - \sqrt{2}kRy}{R\sqrt{\left[-D - R + \sqrt{R^2 - (y - \sqrt{2}kR)^2}\right]^2 + \left(\frac{y - \sqrt{2}kR}{R}\right)^2}} \end{aligned} \right\} \quad (8)$$

$k = 0, \pm 1, \pm 2 \dots$

Substituting formula (8) and (4) into (5), we obtained the theoretical formula for the blast wave overpressure distribution on the oncoming blast surface of a rigid honeycomb wall.

3. NUMERICAL SIMULATION OF OVERPRESSURE BLAST LOAD AGAINST THE HONEYCOMB RIGID WALL BASED ON LS/DYNA

LS/DYNA was used to numerically calculate the blast wave overpressure distribution on the blast surface. For better

comparison with the theoretical model established above, the measuring points on the blast surface of the wall were set, as shown in Figure 3. In the numerical calculation, a 3kg TNT explosive was detonated spherically on the ground. The explosion center was in front of the horizontally symmetrical central axis of the honeycomb wall, and 2.0m from the wall in the horizontal direction.

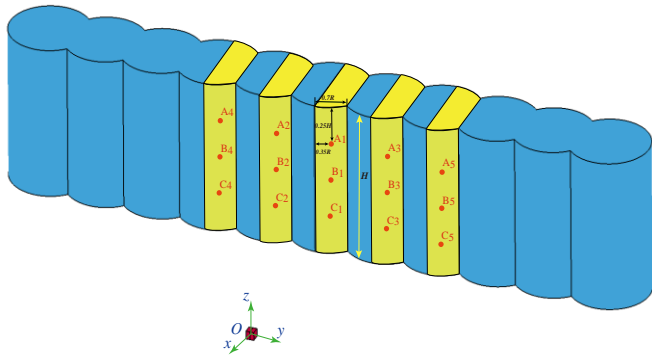


Figure 3. Measuring points of peak overpressure on the circular cross-section blast wall

In LS-DYNA, the *MAT_HIGH_EXPLOSIVE_BURN material model was used as the constitutive model of TNT explosives, and the *EOS_JWL state equation was to simulate

the relationship between the TNT detonation wave front pressure and the initial relative volume V_0 /the internal energy E_0 per unit volume. The ignition time of each TNT unit during explosion is determined by the distance from the centroid of the unit to the detonation point and the detonation velocity. Table 1 lists the explosive materials and the physical and mechanical parameters of the state equation. The air model was simplified as a non-viscous ideal gas, and the expansion of the blast wave was assumed to be an adiabatic process. The air constitutive model used No. 9 material *MAT_NULL. The relationship between blast wave pressure and air initial internal energy density was described by the linear polynomial state equation *EOS_LINEAR_POLYNOMIAL, as shown in Equation (9).

$$P_a = C_0 + C_1\mu + C_2\mu^2 + C_3\mu^3 + (C_4 + C_5\mu + C_6\mu^2)E_{a0} \quad (9)$$

where, P_a is the air blast wave pressure; E_{a0} is the initial internal energy per unit volume; parameters $C_0 = C_1 = C_2 = C_3 = C_6 = 0$, $C_4 = C_5 = \gamma - 1$. The material constitutive and state equation parameters of air are shown in Table 2.

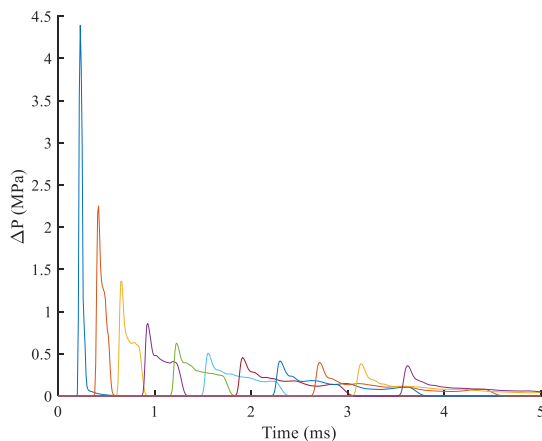
$$P = A \left(1 - \frac{\omega}{R_1 V_0} \right) e^{-R_1 V_0} + B \left(1 - \frac{\omega}{R_2 V_0} \right) e^{-R_2 V_0} + \frac{\omega E_0}{V_0} \quad (10)$$

Table 1. TNT explosive materials and JWL equation parameters

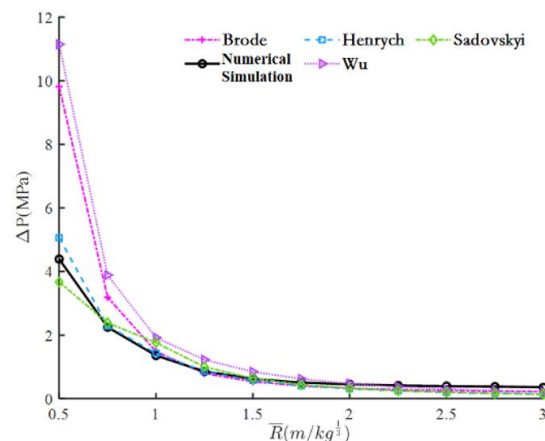
Density of explosives (kg/m ³)	C-J (GPa)	Detonation velocity (m/s)	A (GPa)	B (GPa)	ω	R ₁	R ₂
1630	21.0	6930	371	3.2	0.3	4.2	0.9

Table 2. Air materials and state equation parameters

Density (kg/m ³)	Dynamic viscosity μ (10 ⁻⁵ Pa*s)	Initial pressure (MPa)	Adiabatic index γ
1.29	1.86	0.101	1.4



(a) Free field overpressure time-history curve (scaled distance of explosives $R=0.5\sim 3.0$)



(b) Variation of peak pressure with scaled distance of explosives

Figure 4. Validation of grid accuracy of FEA model for blast field

Figure 4(a) shows the simulated overpressure time-history curve of the free field blast wave at the scaled distance of explosives $R=0.5\sim 3.0$ when the grid density of the finite element model was 3cm under the explosion condition of TNT cylindrical charge. Figure 4(b) shows the variation of the peak overpressure of the free-field blast wave with the scaled distance, and compares with the empirical formula.

It can be seen from Figure 4(b) that with the scaled distance of explosives $\bar{R} < 1$, the results of the blast wave peak overpressure predicted by the empirical formulas have a larger error, and at $\bar{R} \geq 1$, the predicted results are relatively similar. The main reasons are as follows:

1) The peak overpressure data of blast wave is relatively discrete, especially in the vicinity of the explosion;

2) The related experiments were conducted in the last century, and the test results were greatly affected by the accuracy of the sensor and the sampling frequency (and instrument error) of the data acquisition instrument at that time [19, 20].

Figure 4(b) also shows that the numerical simulation results fit well with the empirical formula in a large range of scaled distance, especially in the case of small range ($R < 1.0$), which is basically consistent with Henrych's formula. The numerical calculation results of the air free field blast wave indicate that the simulation parameters and grid division density in this paper can meet the actual needs and calculation accuracy requirements.

Figure 5(a)-(f) depicts the propagation law of the explosion blast wave along the length of the wall (y-axis direction) at the 1/2 height of the blast surface. It can be seen from the figure that at $t=1.98\text{ms}$, the blast wave propagated to the position $y=0$ and was reflected on the blast wall. At this time, the overpressure on the explosion surface increased rapidly at the position of $y=0$, forming the instantaneous bow as shown in (b); while on the cross-section $0 < |y| < \frac{\sqrt{3}}{2}D$, the incident blast wave was regularly reflected, and as $|y|$ increased, the reflected pressure gradually decreased. At $t=2.19\text{ms}$, the explosion blast wave propagated to the cross-section $\frac{\sqrt{3}}{2}D < y < \sqrt{3}D$ of the surface and was reflected, resulting in an

increase in the peak overpressure of the blast wave on the cross-section; comparing with the isobaric cloud diagrams at $t=2.19\text{ms}$ and $t=2.55\text{ms}$, it can be found that the maximum peak pressure appeared near $|y| = \frac{\sqrt{3}}{2}D$ when the explosion blast wave was incident and then reflected/dissipated on the cross-section $\frac{\sqrt{3}}{2}D < y < \sqrt{3}D$, that is, the peak pressure in the cross-sectional area gradually decreased with the $|y|$ increasing. This is mainly due to the superimposed effect of the explosion shock incident wave on the unit cross-sectional area near the concave area and the primary reflected wave on the cross section $0 < |y| < \frac{\sqrt{3}}{2}D$; and in the convex area close to $|y| = \sqrt{3}D$, due to the dissipation of the reflected wave front, the superimposed effect of the primary reflected wave pressure on the cross section is negligible. At the same time, the isobaric cloud diagrams of blast wave from $t=1.45\text{ms}$ to $t=5.0\text{ms}$ showed that when the blast wave front propagated to the blast surface, the blast wave load on the rigid honeycomb wall perpendicular to the direction of the wall gradually changed to a pressure load along the length of the wall (y-axis). This overall concave-convex corrugated cross-section design method can transform the blast load originally perpendicular to the wall into a structural load parallel to the wall, effectively reducing the impact on the wall strength.

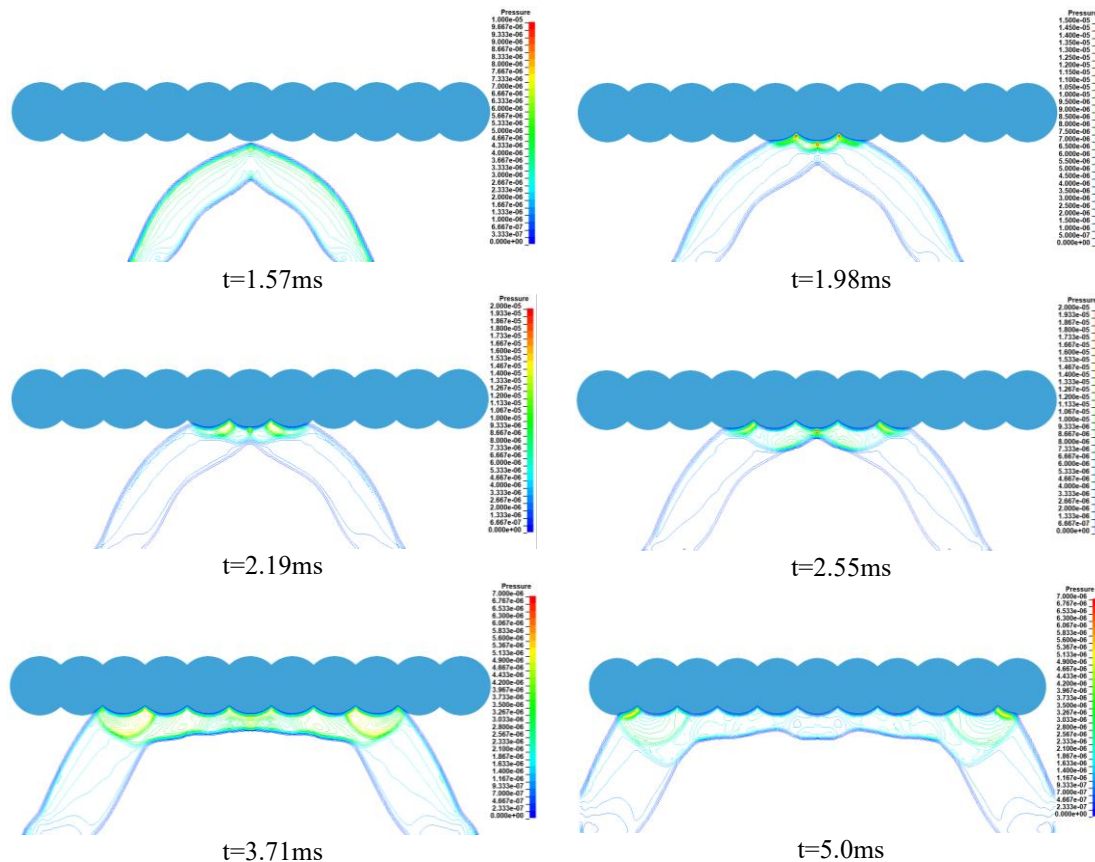


Figure 5. Isobaric cloud diagrams in the height plane of the 1/2 honeycomb wall

Figure 6(a)-(c) respectively show the blast wave peak pressure distribution along the length of the wall at each measuring point A1-A5, B1-B5, and C1-C5 defined in Figure 3. Also, it's compared with the theoretical models of the peak overpressure distribution on the honeycomb rigid wall. The results showed that the peak overpressure at each measuring

point of the honeycomb rigid wall is in the form of sawtooth fluctuations, and gradually decreases as the distance between the measuring points increases along the length of the wall. Comparing the (a) to (c), it's found that the smaller the vertical distance between the measuring point and the bottom of the wall, the better the fitting effect between the equation (5) and

the numerical simulation. Meanwhile, the surface peak overpressure obtained by numerical simulation always tends to be greater than the calculation result of the theoretical model.

This is because the theoretical model does not fully consider the influence of the primary reflection pressure of the adjacent section on the measuring point.

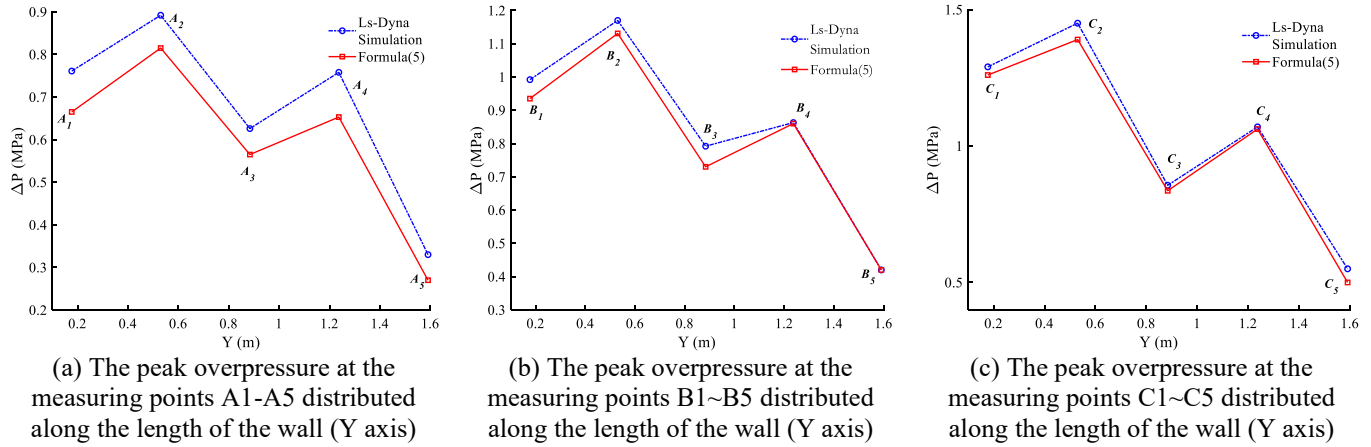


Figure 6. The distribution of peak overpressure at the measuring point of blast load against the honeycomb wall

4. EXPLOSION TEST AND VERIFICATION OF NUMERICAL SIMULATION

The explosion test was carried out in an indoor environment of explosion tower. The explosion tower had an area of about 190m², the tower height of 10m, the tower inner diameter of 8m, and the design explosion equivalent of 2.5kg TNT. Its ground was made of steel plate, which can be considered as no blast wave energy absorption. In the explosion test, the spherical detonation of 300g emulsion explosive was used, and the explosive was placed on the ground 1.0m in front of the central axis of the wall, as shown in Figure 7. Table 3 lists the main parameters of emulsion explosives. For the measurement of wall surface blast wave overpressure, the 137B21X series explosion blast wave measurement sensor produced by PCB Piezotronics was adopted. Table 4 specifies the Technical indicators of PCB blast wave pressure gauges in blast experiment.

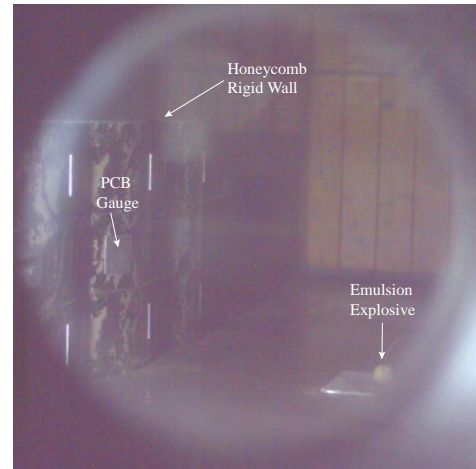


Figure 7. High-speed photograph and site layout of blast experiment

Table 3. Technical indicators of emulsion explosives

Density (g/cm ³)	Minimum brisance (mm)	Minimum detonation velocity (m/s)	Minimum detonation distance (cm)	Minimum blasting force (ml)	TNT equivalent Conversion coefficient
1.2	14	4200	3.0	280.0	0.67

Table 4. Technical indicators of PCB blast wave pressure sensor

Measurement Range (for ±5V output)	Useful Overrange (for ±10V output)	Sensitivity (± 15 %)	Maximum Pressure	Resolution	Rise Time (Incident)	Non-Linearity
345kPa	690kPa	14.5mV/kPa	6895kPa	0.069kPa	<6.5us	<1.0%FS

Before the test, 9 sets of blast wave measuring points G1-G9 were arranged on the honeycomb rigid wall, as shown in Figure 8(b). For the convenience of comparison, three groups of free-field blast wave measuring points ZY_P1~ZY_P3 were also set up in the explosion field, and the horizontal distances from the explosion center were 2.5m, 3.0m and 3.5m respectively, as shown in Figure 8(a). The vertical height of the blast wave sensor from the ground was 0.8m.

Figure 9 shows the blast wave pressure time-history curve at the three free measuring points ZY_P1~ZY_P3. Table 5 lists the peak overpressure values measured by blast wave

sensors at 9 sets of measuring points on the blast surface G1~G9 of the honeycomb rigid wall. Among them, G6 and G8 measuring points failed to collect effective data due to the destructed sensor. The results of the blast wave pressure measured in the explosion test showed that the blast wave overpressure distribution of the rigid honeycomb wall is different from that of the regular rectangular section wall in the ground explosion; the blast wave along the length of the wall doesn't present a monotonous decay trend. Based on the theoretical model of the honeycomb rigid wall established in the previous section, the numerical solution of the peak

overpressure of blast wave at each measuring point G1~G9 was simulated under the same explosion source conditions using numerical calculation method. The experimental data and the LS-DYNA finite element simulation results show that

the FEA results of the explosion blast wave field are in line with the experimental results, verifying the accuracy of the FEA model.

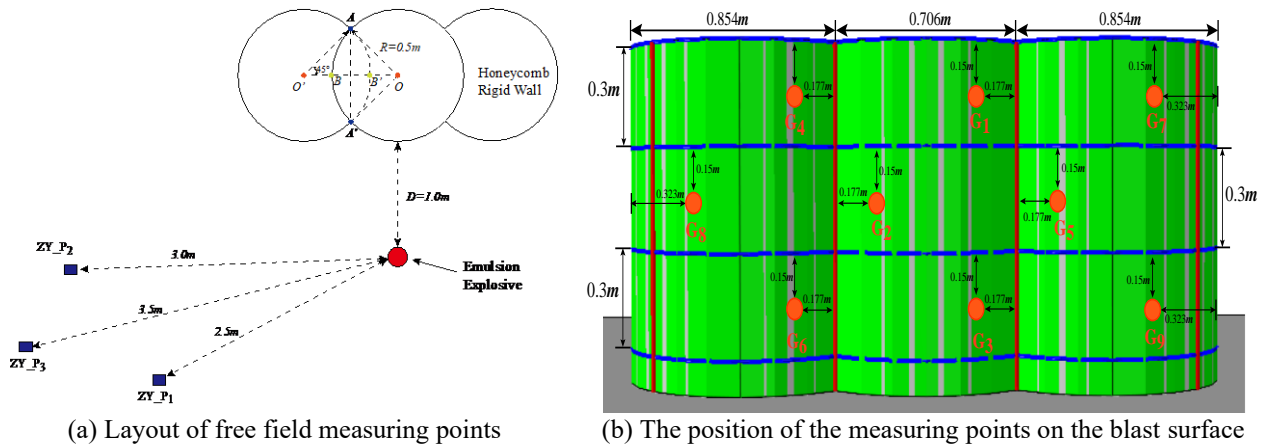


Figure 8. Layout of the measuring points in the explosion test

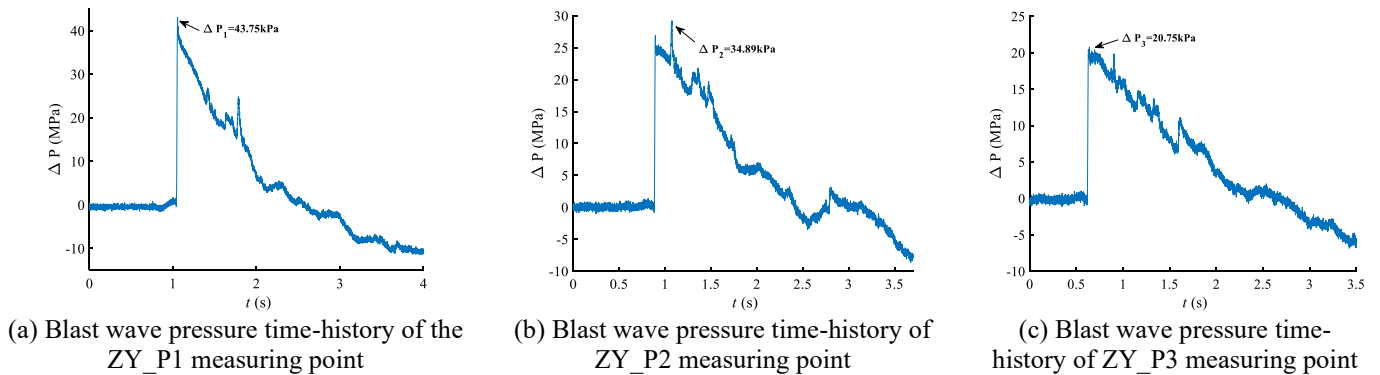


Figure 9. The blast wave time-history data of measuring points in free field

Table 5. Actual explosion test results of each measuring point

Gauge No.	G ₁	G ₂	G ₃	G ₄	G ₅	G ₆
Simulated Pressure (kPa)	662.61	816.45	777.58	663.82	791.54	715.51
Measured Pressure (kPa)	664.25	915.46	713.12	706.82	737.97	---
Gauge No.	G ₇	G ₈	G ₉	ZY P ₁	ZY P ₂	ZY P ₃
Simulated Pressure (kPa)	320.49	363.42	377.16	52.14	33.25	24.73
Measured Pressure (kPa)	205.22	---	241.39	43.75	34.89	20.75

5. CONCLUSIONS

This paper first establishes the theoretical model of the blast wave overpressure distribution on the blast surface of the honeycomb rigid wall. Then, the LS-DYNA numerical finite element analysis method was used to simulate the propagation law of the ground explosion blast wave against the honeycomb section along the length of the wall, and discuss the influence of the wall section shape on the blast wave propagation and attenuation process. Based on the numerical simulation results, the blast wave overpressure distribution law obtained from the theoretical analysis was verified. Finally, the ground explosion test was carried out, to measure the blast wave propagation law of honeycomb wall, and test the blast wave overpressure distribution at the main measuring points of the explosion face, which verifies the FEA model of the honeycomb wall and the propagation law. The main conclusions are as follows:

- (1) The actual explosion test shows that the distribution of blast wave overpressure on the honeycomb wall along the length of the wall presents a non-monotonic change, and the blast wave load distribution on the blast face of the honeycomb wall should not be estimated using the regular reflection empirical formula of blast wave.
- (2) The finite element simulation analysis of the explosion blast wave field shows that the incident angle of the blast face of the honeycomb wall periodically changes with the longitudinal direction of the wall, so that the peak overpressure presents the sawtooth wave form and gradually decreases with the distance of the measuring point along the length of the wall increasing.
- (3) The theoretical model of overpressure distribution on the blast surface of the honeycomb wall based on theoretical analysis can reasonably reveal the pressure load distribution law on the blast surface of the honeycomb rigid wall.

REFERENCE

- [1] Ngo, T., Mendis, P., Gupta, A., Ramsay, J. (2007). Blast loading and blast effects on structures-an overview. *Electronic Journal of Structural Engineering*, 7(S1): 76-91.
- [2] Wu, C., Hao, H. (2005). Modeling of simultaneous ground shock and airblast pressure on nearby structures from surface explosions. *International Journal of Impact Engineering*, 31(6): 699-717. <https://doi.org/10.1016/j.ijimpeng.2004.03.002>
- [3] Rigby, S.E., Tyas, A., Bennett, T., Clarke, S.D., Fay, S.D. (2014). The negative phase of the blast load. *International Journal of Protective Structures*, 5(1): 1-19. <https://doi.org/10.1260/2041-4196.5.1.1>
- [4] Rigby, S.E., Tyas, A., Bennett, T. (2012). Single-degree-of-freedom response of finite targets subjected to blast loading-the influence of clearing. *Engineering Structures*, 45: 396-404. <https://doi.org/10.1016/j.engstruct.2012.06.034>
- [5] Rigby, S.E., Tyas, A., Bennett, T. (2014). Elastic-plastic response of plates subjected to cleared blast loads. *International Journal of Impact Engineering*, 66: 37-47. <https://doi.org/10.1016/j.ijimpeng.2013.12.006>
- [6] Shoja, A., Adabi, M.A., Ahmadnia, M., Zamani, J. (2014). The effect of the relief wave on the uniformity of an air blast load. *Propellants, Explosives, Pyrotechnics*, 39(4): 574-579. <https://doi.org/10.1002/prep.201300094>
- [7] Qasrawi, Y., Heffernan, P.J. (2016). Improved procedure for calculating the cleared pressure acting on a finite target due to a mid-field blast. *International Journal of Protective Structures*, 7(3): 305-324. <https://doi.org/10.1177/2041419616666339>
- [8] Rose, T. A., Smith, P. D., & May, J. H. (2006). The interaction of oblique blast waves with buildings. *Shock Waves*, 16(1): 35-44. <https://doi.org/10.1007/s00193-006-0051-0>
- [9] Tyas, A., Warren, J.A., Bennett, T., Fay, S. (2011). Prediction of clearing effects in far-field blast loading of finite targets. *Shock Waves*, 21(2): 111-119. <https://doi.org/10.1007/s00193-011-0308-0>
- [10] Tyas, A., Bennett, T., Warren, J.A., Fay, S.D., Rigby, S.E. (2011). Clearing of blast waves on finite-sized targets-an overlooked approach. *Applied Mechanics and Materials*, 82: 669-674. <https://doi.org/10.4028/www.scientific.net/AMM.82.669>
- [11] Tyas, A., Rigby, S.E., Clarke, S.D. (2016). Preface to special edition on blast load characterisation. *International Journal of Protective Structures*, 7(3): 303-304. <https://doi.org/10.1177/2041419616666340>
- [12] Rigby, S.E., Tyas, A., Bennett, T., Fay, S.D., Clarke, S.D., Warren, J.A. (2014). A numerical investigation of blast loading and clearing on small targets. *International Journal of Protective Structures*, 5(3): 253-274. <https://doi.org/10.1260/2041-4196.5.3.253>
- [13] Rickman, D.D., Murrell, D.W. (2005). Development of an improved methodology for predicting airblast pressure relief on a directly-loaded wall. *ASME Pressure Vessels and Piping Conference*, 41898: 755-766. <https://doi.org/10.1115/PVP2005-71127>
- [14] Shi, Y., Hao, H., Li, Z.X. (2007). Numerical simulation of blast wave interaction with structure columns. *Shock Waves*, 17(1-2): 113-133. <https://doi.org/10.1007/s00193-007-0099-5>
- [15] Williams, G.D., Williamson, E.B. (2012). Procedure for predicting blast loads acting on bridge columns. *Journal of Bridge Engineering*, 17(3): 490-499. [http://dx.doi.org/10.1061/\(ASCE\)BE.1943-5592.0000265](http://dx.doi.org/10.1061/(ASCE)BE.1943-5592.0000265)
- [16] Liu, H., Torres, D. M., Agrawal, A. K., Yi, Z., Liu, G. (2015). Simplified blast-load effects on the column and bent beam of highway bridges. *Journal of Bridge Engineering*, 20(10): 06015001. [http://dx.doi.org/10.1061/\(ASCE\)BE.1943-5592.0000738](http://dx.doi.org/10.1061/(ASCE)BE.1943-5592.0000738)
- [17] Kingery, C.N., Bulmash, G. (1984). *Airblast Parameters from TNT Spherical Air Burst and Hemispherical Surface Burst Technical Report ARBRL-TR-02555*. MD: U.S. Army Ballistic Research Laboratory, Aberdeen Proving Ground.
- [18] Randers-Pehrson, G., Bannister, K.A. (1997). *Airblast loading model for DYNA2D and DYNA3D ARL-TR-1310*. Adelphi, MD, USA: Army Research Laboratory.
- [19] Brode, H.L. (1959). Blast wave from a spherical charge. *The Physics of Fluids*, 2(2): 217-229. <https://doi.org/10.1063/1.1705911>
- [20] Sadovskyi, M.A. (1952). Mechanical action of air shock waves of explosion, based on experimental data. *Izd Akad Nauk SSSR, Moscow*.